

A fast neural hybrid Newton solver adapted to implicit methods for nonlinear dynamics

Tianyu Jin^{a,c,*}, Georg Maierhofer^b, Katharina Schratz^c, Yang Xiang^{a,d}

^a*Department of Mathematics, The Hong Kong University of Science and Technology, Clear Water Bay, Hong Kong Special Administrative Region of China*

^b*Mathematical Institute, University of Oxford, United Kingdom*

^c*Laboratoire Jacques-Louis Lions (UMR 7598), Sorbonne Université, France*

^d*Algorithms of Machine Learning and Autonomous Driving Research Lab, HKUST Shenzhen-Hong Kong Collaborative Innovation Research Institute, Futian, Shenzhen, China*

Abstract

The use of implicit time-stepping schemes for the numerical approximation of solutions to stiff nonlinear time-evolution equations brings well-known advantages including, typically, better stability behaviour and corresponding support of larger time steps, and better structure preservation properties. However, this comes at the price of having to solve a nonlinear equation at every time step of the numerical scheme. In this work, we propose a novel operator learning based hybrid Newton's method to accelerate this solution of the nonlinear time step system for stiff time-evolution nonlinear equations. We propose a targeted learning strategy which facilitates robust unsupervised learning in an offline phase and provides a highly efficient initialisation for the Newton iteration leading to consistent acceleration of Newton's method. A quantifiable rate of improvement in Newton's method achieved by improved initialisation is provided and we analyse the upper bound of the generalisation error of our unsupervised learning strategy. These theoretical results are supported by extensive numerical results, demonstrating the efficiency of our proposed neural hybrid solver both in one- and two-dimensional cases.

Keywords: implicit method, operator learning, Newton's method, generalisation error

*Corresponding author

Email address: `tjinac@connect.ust.hk` (Tianyu Jin)

1. Introduction

We consider the numerical approximation of solutions to stiff nonlinear time-evolution partial differential equations (PDEs) with implicit numerical methods. In particular, the type of equation we consider in this manuscript is of the following general form with appropriate boundary conditions (e.g. periodic, homogeneous Neumann or Dirichlet)

$$\begin{cases} \partial_t u = Au + f(u), \mathbf{x} \in \Omega, t \in [0, T], \\ u(\mathbf{x}, 0) = u_0(\mathbf{x}), \mathbf{x} \in \overline{\Omega}, \end{cases} \quad (1)$$

where $\Omega \subset \mathbb{R}^d (d = 1, 2, 3)$ is an open and bounded domain, $u : \overline{\Omega} \times [0, T] \rightarrow \mathbb{R}$ is the unknown function, A is a stiff spatial differential operator which causes the stiffness and $f : \mathbb{R} \rightarrow \mathbb{R}$ is a nonlinear function. For our purposes ‘stiff’ in this context will refer to high order spatial derivative operators that inherently require implicit time-steppers to overcome stability issues [1].

While the stiff nature of (1) makes this problem generally challenging, over the last few decades a wide range of successful numerical methods for the approximate solution of (1) have been developed. Explicit methods, while often simpler and more computationally efficient, are typically conditionally stable. For example, a necessary condition, now known as the CFL condition [2], needs to be satisfied for the convergence of the explicit finite difference schemes. On the other hand, implicit methods, and in particular fully implicit methods, are generally unconditionally stable. This implies that they are usually more stable and have better structure-preserving property with wider choice of time step or space increment [1]. Nevertheless, some iterative methods are required in solving fully implicit methods at each time step, which makes them more computationally expensive than explicit methods.

A multitude of iterative methods exist for the resolution of systems of nonlinear equations, each with their unique characteristics and applications. Fixed-point iteration, for instance, is the simplest one while the strong convergence requirement restricts its usage. Picard iteration is another commonly used approach by successively approximating the solution as an integral involving the unknown function. Among all the iterative methods, Newton iteration is a powerful technique with robustness and quadratic convergence rate. However, the evaluation of the Jacobian matrix is indispensable

within each iteration of Newton’s method, thereby causes substantial computational cost. Furthermore, it is noteworthy that Newton’s method exhibits high sensitivity to the initial guess (see Section 3.1 for detailed explanation), as an initial guess that is far from the true solution may result in failure to converge. Hence, there arise two key challenges for improving Newton’s method: (1) mitigating the computational cost, and (2) devising strategies to obtain a ”good” initial guess. Several conventional approaches have been developed to address the first challenge. Quasi-Newton methods [3, 4] are a class of methods based on establishing an approximation to the Jacobian matrix using successive iterates and function values. However, compared to Newton’s method, quasi-Newton methods generally require a larger iteration count. Thus, the cost of these extra iterations is usually higher than the savings in approximating Jacobian per iteration. Another comparable class of methods are so-called inexact Newton methods, originally proposed in [5], which do not require the exact computation of each Newton iterate and instead allow for a small error at each iteration (for example caused by iterative solvers for the corresponding linear Newton-system) by introducing a relative residual into the Newton equation. A notable limitation of inexact Newton methods lies in the constant trade-off between the accuracy needed to maintain Newton iteration’s convergence rate and the computational cost per iteration. This implies that although a large tolerance of error due to residuals can decrease the computational cost per iteration, it may lead to an increase of total iteration count because of the lower convergence rate. Later on, other methods are also proposed based on these two classes of methods. One example is the Newton-Krylov-Schwarz solver [6] for the coupled Allen–Cahn/Cahn–Hilliard system, which combines the inexact Newton iteration with an additive Schwarz preconditioner to enhance computational efficiency. However, choosing proper boundary conditions for the subdomain problems has a huge impact on the convergence of the Schwarz preconditioner. Hence, this method is problem-specific and has some difficulty in dealing with other problems.

In the last decade, deep learning has gained considerable success across various areas of science and engineering, especially in solving PDEs. One notable advancement in this area is operator learning [7, 8, 9, 10], i.e., using the neural network to approximate the mappings between two infinite-dimensional function spaces. Although operator learning exhibits better generalisation property compared to directly learning the unknown function, it still suffers from the problem of non-guaranteed convergence for approxi-

mated solutions, unlike conventional numerical methods. As the time step and the spatial increment tend to 0, the error of the neural network approximated solution does not converge to 0. As a result, it would be more advantageous to combine deep learning methods with classical numerical methods in order to maximize the benefits of both. Continuing to discuss Newton’s method mentioned earlier, there are former works use deep learning methods to improve the original Newton’s method. [11] proposed a nonlinearly preconditioned inexact Newton method with learning capability where a PCA-based unsupervised learning strategy is employed to learn a decomposition in constructing preconditioner. It would also be possible to address the second challenge of Newton’s method by using operator learning methods due to their acceptable accuracy regardless of the time step. In [12, 13], Fourier Neural Operator (FNO) is trained as a time stepper to give a better initial guess in Newton’s method for solving different nonlinear systems of equations. However, training FNO requires a large amount of labeled data, which is often expensive to acquire. Furthermore, generating predictions using FNO typically demands more CPU time compared to traditional neural networks due to the inclusion of the Fast Fourier Transform (FFT) operator. Therefore, the challenge of efficiently training a neural network to furnish a better initial guess in Newton iteration emerges as a significant problem.

In this work, we propose a general neural hybrid solver for a class of stiff nonlinear time-evolution equations. Unlike the supervised learning strategy used in [12, 13], an implicit-scheme-informed unsupervised learning method is constructed to train our neural time stepper with extremely simple and light structure compared to most other operator learning methods. Then the output of the neural network is used as the initial guess in Newton’s method, which can decrease the total iteration count and accelerate the whole algorithm in solving (1) with relatively large time step. Notice that once the neural time stepper is trained, it can consistently provide a ”good” initial guess in multiple time steps until equilibrium without being trained again. We evaluate the proposed method on the Allen–Cahn equation both in 1- and 2-dimensional cases. In such problems, fully implicit methods usually have better structure-preserving properties than explicit methods but are generally more computationally expensive. Examples of several state-of-the-art implicit methods for this equation which are energy-stable include, [14, 15, 16, 17]. Based on the implicit midpoint method, [?] proposed an implicit step-truncation midpoint method and experimental results indicate its efficiency in solving Allen-Cahn equation. Numerical results demonstrate

that the proposed neural hybrid solver outperforms the classical Newton solvers in terms of computational efficiency. While the hybrid approach taken in this work guarantees that the final output of Newton iterations (provided it converged) inherits the rigorously guaranteed properties of the original implicit scheme, we provide further theoretical bounds on the behaviour of the hybrid Newton method. In particular, we provide quantitative estimates on the effect of an improved initialisation on the iteration count in Newton’s method, results which are found to closely match the behaviour in practice. Moreover, we estimate the generalisation error of our proposed unsupervised learning strategy which can be bounded by the training error and the covering error of the training dataset on the underlying function space. This estimate is comparable to the approach taken recently in [18] but differs since in our case we quantify the generalisation error of an operator while [18] considered essentially a function approximator.

The rest of the paper is structured as follows: in Section 2, we introduce the proposed neural hybrid solver in detail. Section 3 presents the asymptotic iteration count estimation of Newton’s method with exponential decaying initialisation and a theoretical analysis of the generalisation error of the employed unsupervised learning strategy under appropriate assumptions. The numerical implements on solving 1- and 2-dimensional Allen–Cahn equations are shown in Section 4.

2. Neural hybrid Newton solver

In this section, we introduce the proposed neural hybrid method to solve the implicit time-stepper. In order to solve (1), we first divide the time interval $[0, T]$ into sub-intervals $0 = t_0 < t_1 < \dots < t_{N_T} = T$ such that $t_n - t_{n-1} = \tau$ for all $n = 1, 2, \dots, N_T$. Suppose $u^n \in \mathbb{R}^{N^d}$, $u^{n+1} \in \mathbb{R}^{N^d}$ are the approximate solution values at t_n , t_{n+1} under the N^d uniform spatial discretisation. Then we denote the implicit method concerned solving (1) to be

$$u^{n+1} = \Psi_\tau(u^n, u^{n+1}) \quad (2)$$

and we further assume the implicitity is involved in the nonlinear term in the operator Ψ_τ (i.e. fully implicit scheme). Therefore, solving the system of nonlinear equations $u = \Psi_\tau(u^n, u)$ is required at each time step. A natural approach is to use Newton iteration. We start our description by recalling the precise definition of Newton iteration.

Remark 1. To denote a slight abuse of notation, we use Ψ_τ to refer both to its discretised form and to the operator applied to variables considered as continuous functions. This dual usage should be clear from the context in which Ψ_τ is applied. The similar dual usage is applied to u^n . When Ψ_τ is considered as an operator, u^n should also be the function corresponding to the discretised numerical approximation.

2.1. Newton iteration

We define a new operator $G(\mathbf{y}) := \mathbf{y} - \Psi_\tau(u^n, \mathbf{y})$ for all $\mathbf{y} \in \mathbb{R}^{N^d}$ mapping from \mathbb{R}^{N^d} to \mathbb{R}^{N^d} . Then solving the semi-discretised version of (2) is equivalent to solving

$$G(\mathbf{y}) = \mathbf{0}, \quad \mathbf{y} \in \mathbb{R}^{N^d}.$$

The Newton iteration of solving systems of nonlinear equations $G(\mathbf{y}) = \mathbf{0}$ is defined as follows.

Definition 1. Denote $D_{\mathbf{y}}G(\mathbf{y})$ the Jacobian matrix of G and we further assume $D_{\mathbf{y}}G(\mathbf{y}^m)$ exists and is non-singular for each $m = 0, 1, 2, \dots$. Then the recursion defined by

$$\mathbf{y}^{m+1} = \mathbf{y}^m - D_{\mathbf{y}}G(\mathbf{y}^m)^{-1}G(\mathbf{y}^m), \quad m = 0, 1, 2, \dots$$

where $\mathbf{y}^0 \in \mathbb{R}^{N^d}$, is called Newton's method (or Newton iteration) for the system of equations $G(\mathbf{y}) = \mathbf{0}$.

As will become a bit more apparent in Section 3.1 the choice of the initial guess \mathbf{y}^0 is crucial for the success and convergence speed of Newton's method. A direct way is to use u^n as the initial guess. However, if τ is large in (2), the direct initial guess u^n may be far from the final solution u^{n+1} and thus cause a large iteration count or, even worse, prevent Newton's method from converging. In the following, we establish a novel neural time stepper approximating the operator mapping from u^n to u^{n+1} to obtain a better initial guess in Newton's method.

2.2. Neural network architecture

In this subsection, we describe the architecture of the neural network in our method. The network we used is a simplified version of the commonly used convolutional neural network (CNN). Generally speaking, the whole neural network consists of L convolutional layers, with a convolution operator

and a nonlinear activation function inside each of them. Also, the number of channels N_c of each convolution operator is increasing within the first $\lfloor \frac{L}{2} \rfloor$ layers and decreasing within the last $\lfloor \frac{L}{2} \rfloor$ layers, which gives us a structure that is wide in the middle and narrow at the ends.

Before giving the rigorous expression of the network architecture, we first review some basic operations in neural networks. We denote by $X \in \mathbb{R}^{m \times n}$ the input feature of the convolution and by $W \in \mathbb{R}^{k \times l}$ the weight of the convolution with $k \leq m$ and $l \leq n$. We use the notation $W \star X$ to represent the correlation of W and X , which reads as

$$(W \star X)_{i,j} = \sum_{r=1}^k \sum_{s=1}^l W_{r,s} X_{i+r-1,j+s-1}, \quad 1 \leq i \leq m-k+1, 1 \leq j \leq n-l+1.$$

Then the notation $pad(X, p) \in \mathbb{R}^{(m+2p) \times (n+2p)}$ is used to represent the padding operator with padding size p . In our settings, we mainly consider homogeneous Neumann boundary condition. According to the conclusion in [19], we choose the *reflect* padding mode in the convolution operator which has the following form.

$$(pad(X, p))_{i,j} = \begin{cases} X_{i,j} & p+1 \leq i \leq p+m, p+1 \leq j \leq p+n \\ X_{2+p-i, 2+p-j} & 1 \leq i, j \leq p, m+p+1 \leq i \leq m+2p, \\ & m+p+1 \leq j \leq n+2p \end{cases}$$

Finally, let σ denote the nonlinear activation function and $X^{(q)}$ denote the output of the q -th convolutional layer where $X_z^{(q)} \in \mathbb{R}^{m \times n}$ denote the z -th channel of it. Suppose $X^{(q-1)}$ has N_{c1} channels and $X^{(q)}$ has N_{c2} channels. Note that the number of channel should be 1, if $q = 1$ or L . Then the structure of each convolutional layer can be represented as follows.

$$X_z^{(q)} = \sigma \left(\sum_{j=1}^{N_{c1}} W_{j,z}^{(q)} \star pad(X_j^{(q-1)}, p) \oplus b_z^{(q)} \right),$$

with the trainable weights $W_{j,z}^{(q)} \in \mathbb{R}^{k \times l}$, biases $b_z^{(q)} \in \mathbb{R}$ and \oplus denotes component-wise addition. The whole architecture with L convolutional layers is illustrated in Figure 1.

2.3. Implicit-scheme-informed learning: Loss function and optimisation

In this subsection, we introduce the training strategy of the aforementioned simplified CNN denoted by \mathcal{N}_θ . Our target is to find an initial guess

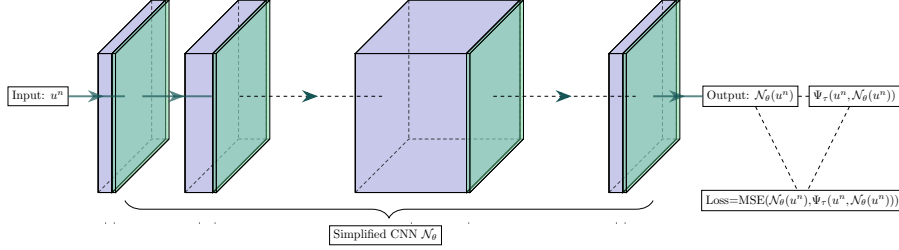


Figure 1: The architecture of the proposed implicit-scheme informed neural network. The purple blocks represent the convolution operator and the green blocks represent the activation function.

as close to u^{n+1} as possible. Thus, we wish the network \mathcal{N}_θ can approximate one step of the implicit scheme (2), i.e. approximate the operator $\Phi_\tau : u^n \mapsto u^{n+1} = \Phi_\tau(u^n)$ for all $n = 0, 1, 2, \dots$. This is achieved by an implicit-scheme-informed unsupervised learning strategy as shown in Figure 1. An abstract paraphrasing of this strategy runs as follows. We define the residual:

$$\mathcal{R}(u) := \Psi_\tau(u^n, u) - u \quad (3)$$

Note that for solution u^{n+1} of (2), $\mathcal{R}(u^{n+1}) = \Psi_\tau(u^n, u^{n+1}) - u^{n+1} \equiv 0$. Assume the input of the network is u^n and $u^n, u^{n+1} \in X$ where X is a function space. The training strategy is to minimize the residual (3) over admissible set of trainable parameters $\theta \in \Theta$, i.e.

$$\text{Find } \theta^* \in \Theta : \quad \theta^* = \arg \min_{\theta \in \Theta} \|\mathcal{R}(\mathcal{N}_\theta(u^n))\|_X \quad (4)$$

Since it is impossible to compute the norm $\|\cdot\|_X$ exactly, we need to approximate it by discretisation. For notational simplicity, we only write the step $u_0 \in X \rightarrow u^1 \in X$ in the loss function without loss of generality. Given a set of initial data $\{u_0^{(i)}\}_{i=1}^{N_{data}}$ as the "quadrature points" in function space X , we determine the parameters $\theta \in \Theta$ via minimising the following loss function as the discrete version of (4):

$$\theta^* = \arg \min_{\theta \in \Theta} \mathcal{L}(\theta) := \arg \min_{\theta \in \Theta} \frac{1}{N_{data}} \sum_{i=1}^{N_{data}} \|\Psi_\tau(u_0^{(i)}, \mathcal{N}_\theta(u_0^{(i)})) - \mathcal{N}_\theta(u_0^{(i)})\|^2. \quad (5)$$

Example 1. *If we work with periodic boundary conditions on the domain $\Omega = [0, 1]^d$ in (1), a sensible choice of $(X, \|\cdot\|)$ would be periodic Sobolev*

spaces with the natural discretisation of the norm arising from a pseudospectral discretisation in space.

In our experiments, the open-source machine learning library PyTorch [20] is used to construct and train the neural network. Following common practice we solve the minimisation problem (5) approximately by stochastic gradient descent, specifically using ADAM [21].

After the neural network is trained, we use the model's prediction, $\mathcal{N}_\theta(u^n)$, as the initial guess in Newton's method. Combined with the recursion of Newton iteration in Definition 1, we summarise our neural hybrid solver in Algorithm 1.

Algorithm 1 Neural hybrid solver for $G(\mathbf{y}) = 0$ (one time step $u^n \rightarrow u^{n+1}$)

```

 $\mathbf{y} = u^n$ 
initialise tolerance  $\epsilon_{tol}$ , length of the update  $l_{update}$  and iteration count  $k$ 
 $\mathbf{y}_{NN} = \mathcal{N}_\theta(\mathbf{y})$ 
for  $i = 1$  to 1000 do
    while  $l_{update} \geq \epsilon_{tol}$  do
        if  $i=1$  then
             $\mathbf{y}_{old} = \mathbf{y}_{NN}$   $\triangleright \mathbf{y}_{NN}$  serves as the initial guess
        else
             $\mathbf{y}_{old} = \mathbf{y}$ 
            calculate  $D_{\mathbf{y}}G(\mathbf{y}_{old})$ ,  $\mathbf{b} = G(\mathbf{y}_{old})$ 
            solve  $\Delta\mathbf{y}$  from  $D_{\mathbf{y}}G(\mathbf{y}_{old})\Delta\mathbf{y} = \mathbf{b}$ 
             $\mathbf{y} = \mathbf{y}_{old} + \Delta\mathbf{y}$ 
             $l_{update} = \|\Delta\mathbf{y}\|_{L^2}$ 
             $k = k + 1$ 
        break
 $u^{n+1} = \mathbf{y}$ 

```

Remark 2. In Algorithm 1, the initial guess \mathbf{y}_{NN} can be replaced by other choices, such as u^n or approximated solution from other numerical methods, to obtain other types of Newton solvers. According to the experimental results presented in Section 4, the neural hybrid solver achieves the best performance among all Newton solvers tested in terms of the trade-off between the computational cost of calculating initial guess and the reduction in iteration

count and, hence, reduction in overall cost of the time-stepper. The GM-RES algorithm can be applied to solve $D_{\mathbf{y}}G(\mathbf{y}_{old})\Delta\mathbf{y} = \mathbf{b}$ after wrapping the matrix-vector multiplication $D_{\mathbf{y}}G(\mathbf{y}_{old})\mathbf{z}, \forall \mathbf{z} \in \mathbb{R}^{N^d}$ into a LinearOperator.

3. Theoretical results

In this section we describe two central theoretical results underpinning our approach for the acceleration of Newton iterations. The first of those results describes specifically the speed-up of the Newton iterations that can be achieved with an improved initialisation. The second result provides a bound on the generalisation error of the neural network, thus ensuring that the accuracy we measure during training extends to relevant unseen data (solution values).

3.1. Asymptotic iteration count estimation of Newton’s method with initialisation

In this part, we provide theoretical results on how much the iteration count can be reduced in Newton’s method (defined in Definition 1) with better initialisation. To begin with, we state some notations and assumptions that will be used later in this subsection. We recall that the system of equations we aim to solve is $G(\mathbf{y}) = \mathbf{0}, \mathbf{y} \in \mathbb{R}^N$ (the general case is $\mathbf{y} \in \mathbb{R}^{N^d}$, but here for notational simplicity we consider $d = 1$ and note that of course the results extend verbatim to the case of $d > 1$). The assumptions on G are summarised in Assumption 1.

Assumption 1. *The system of equations $G(\mathbf{y}) = \mathbf{0}, \mathbf{y} \in \mathbb{R}^N$ satisfies the following two assumptions:*

- (i) *The Jacobian matrix $D_{\mathbf{y}}G$ of G exists and is nonsingular for each element of \mathbf{y} .*
- (ii) *Denote $\boldsymbol{\xi}$ to be the solution of the equation system, i.e. $G(\boldsymbol{\xi}) = \mathbf{0}$. Denote $N_{\text{neighbour}}(\boldsymbol{\xi})$ to be some (open) neighbourhood of $\boldsymbol{\xi}$. In $N_{\text{neighbour}}(\boldsymbol{\xi})$, G is defined and continuous, all the second-order partial derivatives of G are defined and continuous, and $D_{\mathbf{y}}G(\boldsymbol{\xi})$ is nonsingular.*

In the subsequent theorem, we recall the well-known result that Newton’s method (as given in Definition 1) achieves quadratic convergence rate subject to the aforementioned assumptions.

Theorem 1 (Theorem 4.4 in [22]). *Suppose the system of equations $G(\mathbf{y}) = \mathbf{0}$, $\mathbf{y} \in \mathbb{R}^N$ and $N_{\text{neighbour}}(\boldsymbol{\xi})$ satisfy the Assumption 1. Denote the error of the k -th iteration $\varepsilon_k := \|\mathbf{y}^{(k)} - \boldsymbol{\xi}\|_\infty$. Then,*

$$\varepsilon_{k+1} \leq C\varepsilon_k^2,$$

where

$$C = \frac{1}{2}N^2 A_G B_G,$$

$$A_G = \max_{1 \leq i, j, l \leq N} \max_{\mathbf{y} \in \bar{B}_\epsilon(\boldsymbol{\xi})} \left| \frac{\partial^2 G_i}{\partial y_j \partial y_l}(\mathbf{y}) \right|, \quad B_G = \max_{\mathbf{y} \in \bar{B}_\epsilon(\boldsymbol{\xi})} \|[D_{\mathbf{y}} G(\mathbf{y})]^{-1}\|_\infty,$$

for some $\epsilon > 0$ such that $\bar{B}_\epsilon(\boldsymbol{\xi}) \subset N_{\text{neighbour}}(\boldsymbol{\xi})$.

The proof of Theorem 1 can be found in [22]. Using this convergence rate we can now investigate the effect of improving our initial guess ε_0 by a factor of 2^{-n} , $n \in \mathbb{N}$ on the asymptotic iteration count required for convergence in Newton's method.

Theorem 2 (Asymptotic iteration count). *Suppose we are able to improve the initial estimate ε_0 by a factor of 2^{-n} where $n \in \mathbb{N}$. Then the total iteration count, $M = M(n)$, required for Newton's method to achieve a fixed tolerance, asymptotically behaves as follows*

$$M \leq \tilde{C} - \log_2(n) + \mathcal{O}(n^{-1}), \quad \text{as } n \rightarrow \infty,$$

for some constant \tilde{C} which depends on the desired tolerance and the properties of the first- and the second-order partial derivatives of G (i.e. norm of inverse Jacobian and norm of Hessian as outlined above in Theorem 1) but is independent of n .

Proof. From Theorem 1 we have

$$\varepsilon_{k+1} \leq C\varepsilon_k^2 \Rightarrow \varepsilon_k \leq (\varepsilon_0 C)^{2^k} C^{-1}, \quad \text{for } k \geq 0. \quad (6)$$

Suppose we wish to solve the nonlinear system to tolerance $\varepsilon_{\text{tol}} > 0$. Then the total number of iterations required, M is the smallest integer with $\varepsilon_M < \varepsilon_{\text{tol}}$, i.e.

$$M \leq \log_2 |\log_2(\varepsilon_{\text{tol}} C)| - \log_2 |\log_2(\varepsilon_0 C)| + 1. \quad (7)$$

Consider the initial error $\tilde{\varepsilon} = \frac{1}{2^n}\varepsilon_0$ where $n = 0, 1, 2, \dots$, and we replace ε_0 in (7) to be $\tilde{\varepsilon}$. Then we have

$$M \leq \log_2 |\log_2(\varepsilon_{tol}C)| - \log_2 |\log_2(\frac{1}{2^n}\varepsilon_0C)| + 1$$

In the following, we denote $\tilde{C} = \log_2 |\log_2(\varepsilon_{tol}C)| + 1$, then

$$\begin{aligned} M &\leq \tilde{C} - \log_2 | -n + \log_2(\varepsilon_0C) | \\ &= \tilde{C} - \log_2 | 1 - \frac{1}{n} \log_2(\varepsilon_0C) | - \log_2(n) \end{aligned}$$

Thus we find the following asymptotic estimate of M as $n \rightarrow \infty$:

$$\begin{aligned} M &\leq \tilde{C} - \log_2(n) - \log_2 \left| 1 - \frac{1}{n} \log_2(\varepsilon_0C) \right| \\ &= \tilde{C} - \log_2(n) - \frac{1}{n} \log_2(\varepsilon_0C) + \mathcal{O}(n^{-2}), \quad \text{as } n \rightarrow \infty \\ &= \tilde{C} - \log_2(n) + \mathcal{O}(n^{-1}), \quad \text{as } n \rightarrow \infty. \end{aligned}$$

□

Remark 3. We first provide a remark on (6). In (6), the factor $\varepsilon_0^{2^k}$ indicates that a small ε_0 can significantly reduce the error of the k -th step iteration ε_k . Therefore, the importance of initialisation in Newton iteration is demonstrated by this error estimate.

Remark 4. To enhance understanding of Theorem 1, here we provide some comments pertaining to the constant $C = \frac{1}{2}N^2A_GB_G$. We consider solving the Allen–Cahn equation using the midpoint method as described in Section 4. Based on the definitions of A_G and B_G , we find

$$C \propto N^2\tau\|u\|$$

where τ is the time step in the midpoint method and $\|u\|$ is a certain norm of the solution u . Combined with the estimation of total iteration count M in (7), it can be concluded from this proportional relation that (i) larger time steps require a larger amount of Newton iterates; (ii) more spatial discretisation points require a larger amount of Newton iterates.

Remark 5. To further demonstrate our asymptotic estimation in Theorem 2, we investigate the change of iteration count when decreasing the L^2 initial error in Newton iteration with direct initial guess in our numerical examples in Section 4. Figure 2(a) shows the result of the one-dimensional case. The blue line with cross-markers exhibits the true iteration count in the experiment when initial error $\tilde{\varepsilon} = \frac{1}{2^n}\varepsilon_0, n = 0, 1, 2, \dots, 17$. The red dashed line is the graph of $\tilde{C} - \log_2(n)$ as a function of n . Figure 2(b) shows the result of the two-dimensional case. The blue cross line is the iteration count in the experiment when initial error $\tilde{\varepsilon} = \frac{1}{2^n}\varepsilon_0, n = 0, 1, 2, \dots, 12$. Since in the two-dimensional case, the size of the mesh N and also ε_0 are much larger than those in the one-dimensional case, we note that the constant $\log(\varepsilon_0 C)$ is also larger, as observed on the scaling of the axes in this case. From the comparison between the blue and red lines, we find the experiment results are perfectly consistent with our asymptotic estimation both in these two cases.

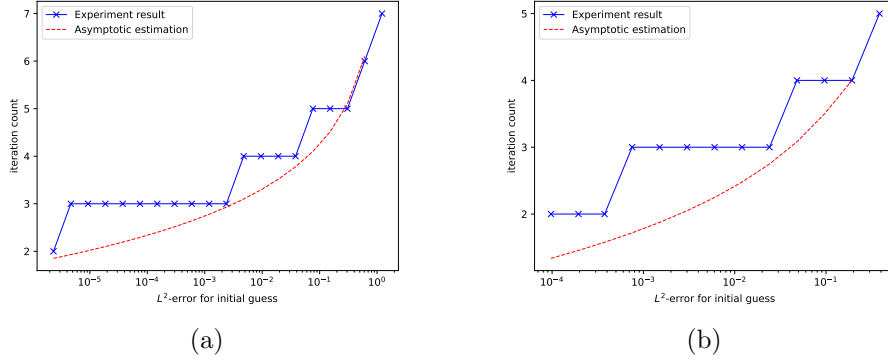


Figure 2: (a) Experimental and asymptotic Newton iteration count in solving 1-dimensional Allen–Cahn equation. The blue cross line is the experiment result, while the red dashed line is the asymptotic estimation; (b) Experimental and asymptotic Newton iteration count in solving 2-dimensional Allen–Cahn equation. The blue cross line is the experiment result, while the red dashed line is the asymptotic estimation.

3.2. Generalisation Error of implicit-scheme-informed Neural Networks

Having studied the cost reduction that can be achieved in Newton’s method using improved initialisations we now turn our attention to understanding how good of an initialisation our neural network approximations

(as described in Section 2) can provide. Our means of understanding the quality of our neural network initialisation will be to study the so-called ‘generalisation error’ which we formally defined in Section 3.2.1. Essentially this quantity provides a measure for how well we expect the initialisation to perform on unseen data, given knowledge of its performance during training. Before we can state the mathematical results more rigorously, we begin with introducing some useful concepts and notation: For a given Banach space X with associated norm $\|\cdot\|_X$ and $z \in X$ we denote by $B_X(z, R)$ the ball of radius R centred at z , i.e.

$$B_X(z, R) = \{z \in X \mid \|z\|_X \leq R\},$$

and we recall from Section 2, that the exact solution of the implicit midpoint rule is denoted by Φ_τ and that our neural network approximation of Φ_τ is given by \mathcal{N}_θ . Recall that the definition of the midpoint rule can be expressed as $\Psi_\tau(u, \Phi_\tau(u)) = \Phi_\tau(u)$. It turns out that a convenient way of studying the generalisation error for tensor product domains ($\Omega = \mathbb{T}^d = [-\pi, \pi]^d$) is via the framework of periodic Sobolev spaces and appropriate subspaces for periodic, Dirichlet and Neumann boundary conditions respectively. In particular, for equations (1) with periodic boundary conditions we consider the Hilbert spaces

$$H_{\text{per}}^s(\Omega) := \{u \in L^2(\Omega) \mid \|u\|_{H_{\text{per}}^s} < \infty\},$$

where the periodic Sobolev norm is defined in the usual way. Given the Fourier coefficients

$$\hat{u}_{\mathbf{k}} = \frac{1}{(2\pi)^d} \int_{\Omega} u(x) e^{-i\mathbf{k} \cdot x} dx,$$

we define

$$\|u\|_{H_{\text{per}}^s}^2 := \sum_{\mathbf{k} \in \mathbb{Z}^d} \langle \mathbf{k} \rangle^{2s} |\hat{u}_{\mathbf{k}}|^2, \quad \text{where } \langle \mathbf{k} \rangle := \begin{cases} |\mathbf{k}| & \text{if } \mathbf{k} \neq \mathbf{0}, \\ 1 & \text{if } \mathbf{k} = \mathbf{0}. \end{cases}$$

In the following we use H^s to replace H_{per}^s for notational simplicity. There are two central properties of these spaces that we exploit in what follows. The first lemma is the Sobolev embedding theorem which comes from Theorem 6.3 in [23].

Lemma 1. *For any $\alpha > \beta \geq 0$, the following embedding is compact:*

$$H^\alpha \rightarrow H^\beta.$$

And we use the following notation to represent this compact embedding:

$$H^\alpha \Subset H^\beta$$

The second lemma is the well-known bilinear estimate.

Lemma 2. *If $\alpha > d/2$, then for any $f, g \in H^\alpha(\mathbb{T}^d)$ the following inequality holds*

$$\|fg\|_{H^\alpha} \leq C_\alpha \|f\|_{H^\alpha} \|g\|_{H^\alpha}$$

for some constant $C_\alpha > 0$.

In case of Dirichlet boundary conditions let us assume without loss of generality that the domain is $\Omega = [0, \pi]^d$. Then we replace the aforementioned Sobolev spaces on $[-\pi, \pi]^d$ by subspaces arising from the condition

$$\hat{u}_{\mathbf{k}} = (-1)^{\sum_{l=1}^d i_l} \hat{u}_{\mathbf{j}}, \text{ whenever } \mathbf{j}_l = (-1)^{i_l} \mathbf{k}_l, \text{ for some } i_l \in \{0, 1\}, l = 1, \dots, d.$$

This is equivalent to the subspaces spanned by Fourier sine series, i.e. (for $s > d/2$) those subspaces satisfying homogeneous Dirichlet conditions on $[0, \pi]^d$. For homogeneous Neumann conditions on $[0, \pi]^d$ we can proceed analogously by considering those subspaces of $H_{\text{per}}^s([-\pi, \pi]^d)$ consisting of functions which satisfy

$$\hat{u}_{\mathbf{k}} = \hat{u}_{\mathbf{j}}, \text{ whenever } \mathbf{j}_l = (-1)^{i_l} \mathbf{k}_l, \text{ for some } i_l \in \{0, 1\}, l = 1, \dots, d,$$

i.e. subspaces spanned by Fourier cosine series. Clearly both of those choices of subspaces inherit the properties described in Lemmas 1 & 2 allowing us to state and prove analogous results as shown below in the periodic case. In the interest of brevity we will therefore focus on the periodic setting for the rest of this section.

While we expect several of the statements in this section to generalise to a larger setting we choose to present our theoretical analysis for a specific equation and numerical integrator. In particular, we consider the Allen–Cahn equation given as follows

$$\begin{cases} \partial_t u(\mathbf{x}, t) = \varepsilon^2 \Delta u(\mathbf{x}, t) - f(u(\mathbf{x}, t)), t \in [0, T], \mathbf{x} \in \Omega, \\ u(\mathbf{x}, 0) = u_0(\mathbf{x}), \mathbf{x} \in \overline{\Omega}, \end{cases} \quad (8)$$

where $\Omega = [-\pi, \pi]^d$ ($d = 1, 2$) (or $\Omega = [0, \pi]^d$ with Dirichlet or homogeneous Neumann boundary conditions), $\varepsilon > 0$ is the interfacial width, and the non-linear function $f(u) = u^3 - u$. Our implicit method of choice for this section

is the implicit midpoint scheme given by

$$u^{n+1} = \Psi_\tau(u^n, u^{n+1}) := u^n + \tau \mathcal{L}\left(\frac{1}{2}(u^n + u^{n+1})\right) \quad (9)$$

where $\mathcal{L}(u) = \varepsilon^2 D_h u - u^3 + u$ and τ is the time step.

Remark 6. *To avoid misunderstanding, we clarify several symbols whose notations appear similar but have different meanings. Specifically, ε refers to the interfacial width, a parameter in Allen-Cahn equation (8). ε_k is the error of the k -th iteration in Newton's method as stated in Theorem 1. On the other hand, ϵ means a small positive number.*

The training of our neural network is performed over a set \mathcal{T} of N_{data} training data points which are, as indicated in Section 2 of specific differentiability and uniformly bounded on the domain of interest, i.e. we assume for all $1 \leq j \leq N_{data}$, $u_j, \Phi_\tau(u_j) \in H^\alpha(\Omega)$ for some $\alpha > d/2$. In particular we sample training data from a bounded ball in $H^\alpha(\Omega)$ which, without loss of generality, we take to be the unit ball for the purposes of this analysis, i.e. $u_j \in B_{H^\alpha}(0, 1)$. From the maximum bound principle (MBP) of the Allen-Cahn equation (see Section 4 for details), it makes sense to choose uniformly bounded training data of the form $u_j \in B_{L^\infty}(0, 1)$. In summary, we will prove an upper bound on the generalisation error for training data of the form

$$\mathcal{T} = \{u_j\}_{j=1}^{N_{data}} \subset B_{H^\alpha}(0, 1) \cap B_{L^\infty}(0, 1), \quad \text{for } \alpha > d/2. \quad (10)$$

3.2.1. Quantifiable estimates on the generalisation error

After training the neural network with the loss (5) we have an automatic control on the training error \mathcal{E}_T , which for mathematical convenience we will express in this section in terms of the maximum over the training dataset \mathcal{T} as given in (10):

$$\mathcal{E}_T = \max_{1 \leq j \leq N_{data}} \|\Psi_\tau(u_j, \Phi_\tau^*(u_j)) - \Phi_\tau^*(u_j)\|_{H^\beta}$$

In the following, we will estimate the error due to our implicit-scheme-informed learning strategy in approximating Φ_τ for unseen data in the relevant set. In particular, we consider the total error over $B_{H^\alpha}(0, 1) \cap B_{L^\infty}(0, 1)$, also referred to as the generalisation error given by:

$$\mathcal{E}_G = \sup_{u \in B_{H^\alpha}(0, 1) \cap B_{L^\infty}(0, 1)} \|\Phi_\tau(u) - \Phi_\tau^*(u)\|_{H^\beta}.$$

In order to make a statement about the generalisation error we assume that the implicit midpoint rule for the Allen–Cahn equations applied to functions of the given regularity has a unique solution. This is similar to Assumption 1 but now in the continuous case.

Assumption 2. *The implicit midpoint scheme always has a unique and bounded solution, i.e. given $u \in H^\alpha$, the solution $\Phi_\tau(u)$ uniquely exists and is bounded in $\|\cdot\|_{H^\alpha}$.*

The following main theorem states that for a sufficiently large training dataset, the generalisation error \mathcal{E}_G is arbitrarily close to the training error \mathcal{E}_T .

Theorem 3. *Suppose $\alpha > \beta + 2 > d/2$ and that Assumption 2 is satisfied. Then there exist constants \tilde{C}_1, \tilde{C}_2 and τ_0 such that the following holds. Given $\epsilon > 0$ there is a $N_\epsilon \in \mathbb{N}$ such that for all $N_{data} > N_\epsilon$ we can find a finite sequence of training data $\{u_j\}_{j=1}^{N_{data}}$ such that for all $\tau < \tau_0$ we have the estimate*

$$\mathcal{E}_G \leq \tilde{C}_1 \mathcal{E}_T + \tilde{C}_2 \epsilon.$$

Furthermore, N_ϵ scales no worse than

$$N_\epsilon \lesssim \left\lceil \left(\frac{4}{\epsilon} \right)^{2d(\frac{\epsilon}{2})^{\frac{1}{\beta+2-\alpha}} + d} \right\rceil.$$

Proof. The proof of Theorem 3 can be divided into two parts.

Step 1: We first estimate \mathcal{E}_G in terms of the residual based error

$$\sup_{u \in B_{H^\alpha}(0,1) \cap B_{L^\infty}(0,1)} \|\mathcal{R}(\Phi_\tau^*(u))\|_{H^\beta},$$

where $\mathcal{R}(\Phi_\tau^*(u)) = \Psi_\tau(u, \Phi_\tau^*(u)) - \Phi_\tau^*(u)$ as defined in (3).

For any $u \in B_{H^\alpha}(0,1) \cap B_{L^\infty}(0,1)$, we have the following identity:

$$\Phi_\tau^*(u) - \Phi_\tau(u) = \Psi_\tau(u, \Phi_\tau^*(u)) - \Psi_\tau(u, \Phi_\tau(u)) - \mathcal{R}(\Phi_\tau^*(u)) \quad (11)$$

The implicit midpoint scheme for the Allen–Cahn equation (8) gives the following expression for Ψ_τ :

$$\Psi_\tau(u, v) = u + \tau \varepsilon^2 \Delta \left(\frac{u+v}{2} \right) - \tau \left(\frac{u+v}{2} \right) \left(\frac{1}{4}(u^2 + 2uv + v^2) - 1 \right)$$

Using this and (11) we find

$$\begin{aligned}\Phi_\tau^*(u) - \Phi_\tau(u) &= \frac{\tau}{2}\varepsilon^2\Delta(\Phi_\tau^*(u) - \Phi_\tau(u)) + \frac{\tau}{2}(\Phi_\tau^*(u) - \Phi_\tau(u)) \\ &\quad - \tau \left[\left(\frac{u + \Phi_\tau^*(u)}{2} \right)^3 - \left(\frac{u + \Phi_\tau(u)}{2} \right)^3 \right] \\ &\quad - \mathcal{R}(\Phi_\tau^*(u)).\end{aligned}$$

Thus

$$\begin{aligned}((1 - \frac{\tau}{2})I - \frac{\tau}{2}\varepsilon^2\Delta)(\Phi_\tau^*(u) - \Phi_\tau(u)) &= -\tau \left[\left(\frac{u + \Phi_\tau^*(u)}{2} \right)^3 - \left(\frac{u + \Phi_\tau(u)}{2} \right)^3 \right] \\ &\quad - \mathcal{R}(\Phi_\tau^*(u)).\end{aligned}\tag{12}$$

For $\tau < 2$ we have, due to the spectrum of Δ ,

$$C_{1,\tau} := \|((1 - \frac{\tau}{2})I - \frac{\tau}{2}\varepsilon^2\Delta)^{-1}\|_{H^\beta \rightarrow H^\beta} < \infty.$$

Hence we can perform the following estimate:

$$\begin{aligned}\|\Phi_\tau(u) - \Phi_\tau^*(u)\|_{H^\beta} &\leq C_{1,\tau} \frac{\tau}{8} \|(u + \Phi_\tau^*(u))^3 - (u + \Phi_\tau(u))^3\|_{H^\beta} \\ &\quad + C_{1,\tau} \|\mathcal{R}(\Phi_\tau^*(u))\|_{H^\beta} \\ &= C_{1,\tau} \frac{\tau}{8} \|[(u + \Phi_\tau^*(u))^2 + (u + \Phi_\tau^*(u))(u + \Phi_\tau(u)) \\ &\quad + (u + \Phi_\tau(u))^2](\Phi_\tau^*(u) - \Phi_\tau(u))\|_{H^\beta} \\ &\quad + C_{1,\tau} \|\mathcal{R}(\Phi_\tau^*(u))\|_{H^\beta} \\ &\leq \tau C_2 \|\Phi_\tau^*(u) - \Phi_\tau(u)\|_{H^\beta} + C_{1,\tau} \|\mathcal{R}(\Phi_\tau^*(u))\|_{H^\beta}\end{aligned}$$

where Lemma 2 is used to obtain the last inequality and

$$C_2 := \frac{1}{8}C_{1,\tau}C_\beta \|(u + \Phi_\tau^*(u))^2 + (u + \Phi_\tau^*(u))(u + \Phi_\tau(u)) + (u + \Phi_\tau(u))^2\|_{H^\beta}$$

Observe that our neural network \mathcal{N}_θ is based on linear layers and hyperbolic tangent activation functions. Thus the map Ψ^* is infinitely differentiable and therefore we can bound $\|\Phi_\tau^*(u)\|_{H^\beta}$ in terms of (a smooth function of) $\|u\|_{H^\alpha}$. Similarly to the argument in (12) we also have

$$\Phi_\tau(u) = \frac{(1 + \frac{\tau}{2})I + \frac{\tau\varepsilon^2\Delta}{2}}{(1 - \frac{\tau}{2})I - \frac{\tau\varepsilon^2\Delta}{2}}u - \frac{\tau}{(1 - \frac{\tau}{2})I - \frac{\tau\varepsilon^2\Delta}{2}} \left(\frac{u + \Phi_\tau(u)}{2} \right)^3.$$

Thus, by Assumption 2 we know that for τ sufficiently small $\|\Phi_\tau(u)\|_{H^\beta}$ is bounded in terms of a Lipschitz function of $\|u\|_{H^\beta}$. Moreover, the definition of Sobolev norm implies that $\|u\|_{H^\beta} \leq \|u\|_{H^\alpha} \leq 1$. Thus, C_2 is uniformly bounded for any $u \in B_{H^\alpha}(0,1)$ since $\|\Phi_\tau^*(u)\|_{H^\beta}$, $\|\Phi_\tau(u)\|_{H^\beta}$ and $\|u\|_{H^\beta}$ are all bounded.

We continue to estimate $\|\Phi_\tau(u) - \Phi_\tau^*(u)\|_{H^\beta}$. For $\tau < \frac{1}{C_2}$ we have

$$\|\Phi_\tau(u) - \Phi_\tau^*(u)\|_{H^\beta} \leq \frac{C_{1,\tau}}{1 - \tau C_2} \|\mathcal{R}(\Phi_\tau^*(u))\|_{H^\beta}.$$

The important thing to recall here is that

$$\|\mathcal{R}(\Phi_\tau^*(u))\|_{H^\beta} = \|\Psi_\tau(u, \Phi_\tau^*(u)) - \Phi_\tau^*(u)\|_{H^\beta}.$$

Therefore after taking supremum we have

$$\mathcal{E}_G \leq \sup_{u \in B_{H^\alpha}(0,1) \cap B_{L^\infty}(0,1)} \frac{C_{1,\tau}}{1 - \tau C_2} \|\mathcal{R}(\Phi_\tau^*(u))\|_{H^\beta}.$$

In conclusion, let $\tau_0 = \min\{2, \frac{1}{C_2}\}$ and $\tilde{C} = \frac{C_{1,\tau}}{1 - \tau C_2}$. Then we have the following estimate of generalisation error \mathcal{E}_G in terms of the residual based error, valid for any $0 < \tau < \tau_0$:

$$\mathcal{E}_G \leq \tilde{C} \sup_{u \in B_{H^\alpha}(0,1) \cap B_{L^\infty}(0,1)} \|\mathcal{R}(\Phi_\tau^*(u))\|_{H^\beta}. \quad (13)$$

This completes the first step of the proof.

Step 2: Now we estimate

$$\sup_{u \in B_{H^\alpha}(0,1) \cap B_{L^\infty}(0,1)} \|\mathcal{R}(\Phi_\tau^*(u))\|_{H^\beta}$$

in terms of the training error \mathcal{E}_T .

Since $B_{H^\alpha}(0,1) \cap B_{L^\infty}(0,1)$ is bounded in H^α , combined with the conclusion in Lemma 1 we know $B_{H^\alpha}(0,1) \cap B_{L^\infty}(0,1)$ is totally bounded in $H^{\beta+2}$. Thus for any given $\epsilon > 0$ there is a finite ϵ -net w.r.t. $\|\cdot\|_{H^{\beta+2}}$ covering $B_{H^\alpha}(0,1) \cap B_{L^\infty}(0,1)$. i.e. there is an $N_\epsilon \in \mathbb{N}$ and $u_j \in B_{H^\alpha}(0,1) \cap B_{L^\infty}(0,1)$ for $1 \leq j \leq N_\epsilon$ such that

$$B_{H^\alpha}(0,1) \cap B_{L^\infty}(0,1) \subset \bigcup_{j=1}^{N_\epsilon} B_{H^{\beta+2}}(u_j, \epsilon).$$

An upper bound on the size of N_ϵ is given in Proposition 1. For simplicity of notation, we shall write $B_\cap = B_{H^\alpha}(0, 1) \cap B_{L^\infty}(0, 1)$ in what follows. We now have

$$\sup_{u \in B_\cap} \|\mathcal{R}(\Phi_\tau^*(u))\|_{H^\beta} = \max_{1 \leq j \leq N_\epsilon} \sup_{v \in B_{H^{\beta+2}}(u_j, \epsilon) \cap B_\cap} \|\mathcal{R}(\Phi_\tau^*(v))\|_{H^\beta}$$

Now we have for any $v \in B_{H^{\beta+2}}(u_j, \epsilon)$

$$\|\mathcal{R}(\Phi_\tau^*(v))\|_{H^\beta} \leq \|\mathcal{R}(\Phi_\tau^*(u_j))\|_{H^\beta} + \|\mathcal{R}(\Phi_\tau^*(v)) - \mathcal{R}(\Phi_\tau^*(u_j))\|_{H^\beta}.$$

We note that

$$\begin{aligned} \|\mathcal{R}(\Phi_\tau^*(v)) - \mathcal{R}(\Phi_\tau^*(u_j))\|_{H^\beta} &= \|\Psi_\tau(v, \Phi_\tau^*(v)) - \Phi_\tau^*(v) \\ &\quad - \Psi_\tau(u_j, \Phi_\tau^*(u_j)) + \Phi_\tau^*(u_j)\|_{H^\beta} \\ &\leq \|\Psi_\tau(v, \Phi_\tau^*(v)) - \Psi_\tau(u_j, \Phi_\tau^*(u_j))\|_{H^\beta} \\ &\quad + \|\Phi_\tau^*(v) - \Phi_\tau^*(u_j)\|_{H^\beta} \\ &\stackrel{\text{def}}{=} \text{I} + \text{II} \end{aligned}$$

We first estimate II. Similar to the steps in [25], it is easy to show our neural network is Lipschitz continuous. This means that there is a Lipschitz constant $C_{lip, NN} > 0$ such that

$$\text{II} = \|\Phi_\tau^*(v) - \Phi_\tau^*(u_j)\|_{H^\beta} \leq C_{lip, NN} \|v - u_j\|_{H^\beta}.$$

It remains to estimate I. Notice that

$$\begin{aligned} \text{I} &= \|\Psi_\tau(v, \Phi_\tau^*(v)) - \Psi_\tau(u_j, \Phi_\tau^*(u_j))\|_{H^\beta} \\ &= \|((1 + \frac{\tau}{2})I + \frac{\tau}{2}\varepsilon^2\Delta)(v - u_j) + (\frac{\tau}{2}I + \frac{\tau}{2}\varepsilon^2\Delta)(\Phi_\tau^*(v) - \Phi_\tau^*(u_j)) \\ &\quad - \frac{\tau}{8}[(v + \Phi_\tau^*(v))^2 + (v + \Phi_\tau^*(v))(u_j + \Phi_\tau^*(u_j)) + (u_j + \Phi_\tau^*(u_j))^2] \\ &\quad \cdot (v - u_j + \Phi_\tau^*(v) - \Phi_\tau^*(u_j))\|_{H^\beta} \\ &\leq \|((1 + \frac{\tau}{2})I + \frac{\tau}{2}\varepsilon^2\Delta)(v - u_j)\|_{H^\beta} + \|(\frac{\tau}{2}I + \frac{\tau}{2}\varepsilon^2\Delta)(\Phi_\tau^*(v) - \Phi_\tau^*(u_j))\|_{H^\beta} \\ &\quad + \frac{\tau}{8}C_\beta \|(v + \Phi_\tau^*(v))^2 + (v + \Phi_\tau^*(v))(u_j + \Phi_\tau^*(u_j)) + (u_j + \Phi_\tau^*(u_j))^2\|_{H^\beta} \\ &\quad \cdot \|v - u_j + \Phi_\tau^*(v) - \Phi_\tau^*(u_j)\|_{H^\beta} \end{aligned}$$

Lemma 2 is used to obtain the last inequality. We now note that

$$\|\Delta u\|_{H^\beta} \leq \|u\|_{H^{\beta+2}} \leq \|u\|_{H^\alpha}.$$

Also, from the fact that $\|v\|_{H^\beta}, \|u_j\|_{H^\beta}, \|\Phi_\tau^*(v)\|_{H^\beta}$ and $\|\Phi_\tau^*(u_j)\|_{H^\beta}$ are all bounded, we can introduce another constant C_3 which is uniformly bounded for $u_j \in B_{H^\alpha}(0, 1)$:

$$C_3 = \|(v + \Phi_\tau^*(v))^2 + (v + \Phi_\tau^*(v))(u_j + \Phi_\tau^*(u_j)) + (u_j + \Phi_\tau^*(u_j))^2\|_{H^\beta}.$$

Substituting this into the estimate of I yields

$$\begin{aligned} \text{I} &\leq (1 + \frac{\tau}{2} + \frac{\tau}{2}\varepsilon^2)\|v - u_j\|_{H^{\beta+2}} + (\frac{\tau}{2} + \frac{\tau}{2}\varepsilon^2)C_{lip,NN}\|v - u_j\|_{H^{\beta+2}} \\ &\quad + \frac{\tau}{8}C_\beta C_3(1 + C_{lip,NN})\|v - u_j\|_{H^\beta} \\ &\leq C_4\|v - u_j\|_{H^{\beta+2}}, \end{aligned}$$

where $C_4 = 1 + \frac{\tau}{2} + \frac{\tau}{2}\varepsilon^2 + (\frac{\tau}{2} + \frac{\tau}{2}\varepsilon^2)C_{lip,NN} + \frac{\tau}{8}C_\beta C_3(1 + C_{lip,NN})$. Therefore, the estimates of I and II lead to

$$\|\mathcal{R}(\Phi_\tau^*(v)) - \mathcal{R}(\Phi_\tau^*(u_j))\|_{H^\beta} \leq (C_{lip,NN} + C_4)\|v - u_j\|_{H^{\beta+2}} \leq C_5\epsilon$$

where $C_5 = C_{lip,NN} + C_4$. It follows that

$$\|\mathcal{R}(\Phi_\tau^*(v))\|_{H^\beta} \leq \|\mathcal{R}(\Phi_\tau^*(u_j))\|_{H^\beta} + C_5\epsilon$$

It follows immediately by taking supremum over B_\cap that

$$\begin{aligned} \sup_{u \in B_\cap} \|\mathcal{R}(\Phi_\tau^*(u))\|_{H^\beta} &= \max_{1 \leq j \leq N_\epsilon} \sup_{v \in B_{H^{\beta+2}}(u_j, \epsilon) \cap B_\cap} \|\mathcal{R}(\Phi_\tau^*(v))\|_{H^\beta} + C_5\epsilon \\ &\leq \max_{1 \leq j \leq N_\epsilon} \|\mathcal{R}(\Phi_\tau^*(u_j))\|_{H^\beta} + C_5\epsilon \\ &= \mathcal{E}_T + C_5\epsilon. \end{aligned} \tag{14}$$

This completes Step 2. Finally, we can combine (13) and (14) to estimate

$$\begin{aligned} \mathcal{E}_G &\leq \tilde{C}_1 \sup_{u \in B_\cap} \|\mathcal{R}(\Phi_\tau^*(u))\|_{H^\beta} + \tilde{C}_1 C_5\epsilon \\ &\leq \tilde{C}_1 \mathcal{E}_T + \tilde{C}_2\epsilon \end{aligned}$$

where $\tilde{C}_2 = \tilde{C}_1 C_5$. This concludes the proof. \square

3.2.2. Minimal number of training data required

We then investigate how much training data are required in order to achieve the accuracy $\epsilon > 0$. From the the second part of the proof of Theorem 3, we find the amount of training data required is equivalent to the size of an ϵ -net covering $B_{H^\alpha}(0, 1) \cap B_{L^\infty}(0, 1)$ in $H^{\beta+2}$. The following proposition provides a quantifiable estimate on the size of such an ϵ -net.

Proposition 1 (Amount of training data required to achieve ϵ -accuracy.). *Fix $\alpha > \beta + 2 > d/2$. Given $\epsilon > 0$ there is an ϵ -Net of size at most*

$$N_\epsilon = \left\lceil \left(\frac{4}{\epsilon} \right)^{2d(\frac{\epsilon}{2})^{\frac{1}{\beta+2-\alpha}} + d} \right\rceil$$

covering $B_{H^\alpha}(0, 1) \cap B_{L^\infty}(0, 1)$ in $H^{\beta+2}$.

Proof. For a given $N_0 \in \mathbb{N}$ let us denote by \mathcal{P}_{N_0} the following projection

$$\mathcal{P}_{N_0} f = \mathcal{P}_{N_0} \left(\sum_{k^d \in \mathbb{Z}} \hat{f}_k e^{ikx} \right) = \sum_{|k| \leq N_0} \hat{f}_k e^{ikx}, \text{ for any } f \in H^s(\mathbb{T}), s \geq 0,$$

where for a vector $k \in \mathbb{Z}^d$ we write

$$|k| = \sum_{l=1}^d |k_l|, \quad \langle k \rangle = \begin{cases} |k|, & \text{if } k \neq 0, \\ 1, & \text{otherwise.} \end{cases}$$

Then we have for any $u \in B_{H^\alpha}(0, 1) \cap B_{L^\infty}(0, 1)$:

$$\begin{aligned} \|(I - \mathcal{P}_{N_0})u\|_{H^{\beta+2}}^2 &= \sum_{|k| > N_0} \langle k \rangle^{2\beta+4} |\hat{u}_k|^2 \\ &= \sum_{|k| > N_0} \langle k \rangle^{2\beta+4-2\alpha} \langle k \rangle^{2\alpha} |\hat{u}_k|^2 \leq N_0^{2(\beta+2-\alpha)} \|u\|_{H^\alpha}^2 \leq N_0^{2(\beta+2-\alpha)}. \end{aligned}$$

This implies that for $N_0 > (\frac{\epsilon}{2})^{\frac{1}{\beta+2-\alpha}}$

$$\|(I - \mathcal{P}_{N_0})u\|_{H^{\beta+2}} < \epsilon/2. \tag{15}$$

Naturally, the next step would be finding a finite $\frac{\epsilon}{2}$ -net in $H^{\beta+2}$ for the *finite dimensional* space $\mathcal{P}_{N_0}(B_{H^\alpha}(0, 1) \cap B_{L^\infty}(0, 1))$. Since $\|u\|_{H^{\beta+2}} \leq \|u\|_{H^\alpha}$ it thus suffices to find a finite $\frac{\epsilon}{2}$ -net for $\mathcal{P}_{N_0}(B_{H^{\beta+2}}(0, 1))$ in $H^{\beta+2}$. To do so

we construct an isometry that maps $\mathcal{P}_{N_0}(B_{H^{\beta+2}}(0, 1))$ into $\mathbb{R}^{(2N_0+1)d}$ and then rely on standard covering number estimates on Euclidean spaces. Our isometry of choice is the map

$$M : \mathcal{P}_{N_0}(B_{H^{\beta+2}}(0, 1)) \rightarrow \mathbb{R}^{(2N_0+1)d}$$

$$u \mapsto (\langle k \rangle^{\beta+2} \hat{u}_k)_{|k| \leq N_0}$$

Thus it suffices to find an $\frac{\epsilon}{2}$ -net for the ball of radius 1 in $\mathbb{R}^{(2N_0+1)d}$. From the conclusion of Example 27.1 in [24], the smallest size of such a $\frac{\epsilon}{2}$ -net, $N_{\frac{\epsilon}{2}}$, can be bounded as follows

$$N_{\frac{\epsilon}{2}} \leq \left(\frac{4}{\epsilon}\right)^{(2N_0+1)d}.$$

Thus, recalling (15), for any

$$N_\epsilon > \left(\frac{4}{\epsilon}\right)^{(2N_0+1)d} > \left(\frac{4}{\epsilon}\right)^{2d(\frac{\epsilon}{2})^{\frac{1}{\beta+2-\alpha}} + d},$$

we can find $u_1, \dots, u_{N_\epsilon} \in \mathcal{P}_{N_0}(B_{H^\alpha}(0, 1) \cap B_{L^\infty}(0, 1))$ such that for all $u \in B_{H^\alpha}(0, 1) \cap B_{L^\infty}(0, 1)$ there is a $u_j \in \mathcal{P}_{N_0}(B_{H^\alpha}(0, 1) \cap B_{L^\infty}(0, 1))$ as the centre of those $\frac{\epsilon}{2}$ -balls such that

$$\begin{aligned} \|u - u_j\|_{H^{\beta+2}} &\leq \|\mathcal{P}_{N_0}(u - u_j)\|_{H^{\beta+2}} + \|(I - \mathcal{P}_{N_0})(u - u_j)\|_{H^{\beta+2}} \\ &\leq \|\mathcal{P}_{N_0}(u) - u_j\|_{H^{\beta+2}} + \|(I - \mathcal{P}_{N_0})(u)\|_{H^{\beta+2}} \\ &< \frac{\epsilon}{2} + \frac{\epsilon}{2} \\ &= \epsilon. \end{aligned}$$

Therefore, we can conclude that there is a ϵ -net of size at most $\left\lceil \left(\frac{4}{\epsilon}\right)^{2d(\frac{\epsilon}{2})^{\frac{1}{\beta+2-\alpha}} + d} \right\rceil$ covering $B_{H^\alpha}(0, 1) \cap B_{L^\infty}(0, 1)$ in $H^{\beta+2}$. \square

4. Numerical examples and evaluation

Following the theoretical results in previous sections we now provide several numerical experiments to demonstrate the speed-up that can be achieved using our neural hybrid solver to initialise Newton's method. Aligned with

the theoretical analysis in Section 2.3, we consider solving the Allen–Cahn equation (8), a reaction–diffusion equation that describes the motion of a curved antiphase boundary [26], equipped with homogeneous Neumann boundary condition. It is known that equation (8) is the L^2 gradient flow with respect to the following energy functional

$$E(u) = \int_{\Omega} \left(\frac{\varepsilon^2}{2} |\nabla u|^2 + F(u) \right) d\mathbf{x}, \quad (16)$$

where $F(u) = \frac{1}{4}(u^2 - 1)^2$ such that $F'(u) = f(u)$. Observe that

$$\frac{d}{dt} E(u(t)) = - \int_{\Omega} |\partial_t u(\mathbf{x}, t)|^2 d\mathbf{x} \leq 0.$$

Hence, the energy (16) dissipates along the evolution of (8).

Another important property of (8) is that its solution satisfies the maximum bound principle (MBP). Namely if

$$\max_{\mathbf{x} \in \bar{\Omega}} |u_0(\mathbf{x})| \leq 1,$$

then the following also holds

$$\max_{\mathbf{x} \in \bar{\Omega}} |u(\mathbf{x}, t)| \leq 1 \quad \text{for all } t > 0.$$

Energy dissipation and MBP are two vital physical properties of (8). Thus, when constructing numerical methods, we hope to preserve them in order to achieve better long-term behaviour.

Numerous numerical methods are exploited in the literature for solving semilinear parabolic equations like (8). [16] proposed a provably unconditionally stable mixed variational method for the class of phase-field models. However, only the nonlinear stability restricted to the free energy can be guaranteed in this method. [27] explored an MBP-preserving method for the Allen–Cahn equation which uses implicit-explicit scheme in time and central finite difference in space. Exponential-type integrators have been found to have some advantages in solving equations containing strong stiff linear terms. An example of the exponential-type integrators is the exponential time differencing (ETD) schemes studied in [28]. In ETD methods, which are based on Duhamel’s formula, the linear part is evaluated exactly leading to both stability and accuracy. As we noted in Section 1, fully implicit

schemes, such as implicit midpoint methods, often exhibit better stability and accuracy with even relatively large time steps. However, implicit methods are more challenging to employ, due to their high computational cost.

Throughout this section we focus on solving (8) by the implicit midpoint method (9), the most common fully implicit method, in time and using a central finite difference discretisation in space. However, we note that our proposed method provides a general framework of hybrid Newton solvers for implicit numerical methods that is not limited to the present discretisation. As a baseline for judging whether our proposed neural hybrid solver can accelerate the whole time-stepping algorithm and achieve a better performance we compare also against explicit methods, such as the ETD method. Before discussing the numerical results let us provide a few additional details on our implementation. First of all, we write down the central finite difference scheme to approximate the spatial derivatives as shown in [27]. Denote by D_h the discrete matrix of the Laplacian Δ equipped with homogeneous Neumann boundary condition in 1-dimensional case.

$$D_h = \Lambda_h := \frac{1}{h^2} \begin{bmatrix} -1 & 1 & & & \\ 1 & -2 & 1 & & \\ & \ddots & \ddots & \ddots & \\ & & 1 & -2 & 1 \\ & & & 1 & -1 \end{bmatrix}_{N \times N}$$

where h is the spatial increment. Let \otimes denote the Kronecker product and I is the identity matrix, then the discrete matrix of Laplacian in the 2-dimensional case can be written as

$$D_h = I \otimes \Lambda_h + \Lambda_h \otimes I.$$

The implicit midpoint method has been given in (9). The time step τ here is also referred to as $\tau_{midpoint}$ in the following subsections, to distinguish it from parameters in the reference schemes.

The ETD scheme in for the solution of (8) is given as follows.

$$u^{n+1} = e^{\tau A} u^n + \tau \varphi_1(\tau A) f(u^n),$$

where $A = \varepsilon^2 D_h$, $\varphi_1(z) = \frac{1-e^z}{z}$. The time step τ in this scheme is also referred to as τ_{ETD} . To ensure that the ETD method used in our implementations is state-of-the-art, the standard Krylov method is applied to fast

approximate phi-functions as shown in [29]. The training of the neural network was conducted on the Tianhe-2 supercomputer with one GPU core and six CPU cores, while all the remaining parts were performed on a MacBook Air equipped with an Apple M1 chip.

4.1. 1-dimensional example

We first provide a 1-dimensional example where the interfacial width is fixed to $\varepsilon = 0.01$. The space interval $\Omega = [-\pi, \pi] \subset \mathbb{R}$ is discretised into 512 uniform mesh points. The initial data u_0 are generated by

$$u_0 = \sum_{i=1}^{128} a_i e^{-i/4} \sin(ix) + b_i e^{-i/4} \cos(ix) \quad (17)$$

where the coefficients $a_i, b_i \sim \mathcal{N}(0, 1)$ are sampled from a normal distribution. We then normalise the generated data by $u_0 \leftarrow \frac{u_0}{\max(|u_0|)}$ so that $\|u_0\|_{L^\infty} \leq 1$. Using this method, we randomly generate 3520 different initial data and separate them into the training dataset $\{u_0^{(i)}\}_{i=1}^{N=3200}$ and testing dataset $\{u_0^{(i)}\}_{i=1}^{320}$.

The architecture of the neural network is illustrated in Section 2. Here we give more details on the hyperparameter setting in this case. The whole neural network is composed of 8 convolutional layers, each consisting of one *Conv1d* operator and the activation function $\sigma = \text{Tanh}()$. All the *Conv1d* operators in this case have 21 kernel size, 1 stride, and 10 padding with the *reflect* padding mode. Under this setting, a simplified convolutional neural network with 113409 learnable parameters is applied as our model to approximate the implicit midpoint time-stepper (9) with $\tau_{\text{midpoint}} = 0.5, 1, 2$, respectively.

The loss function is defined in (5) and is minimized by the optimizer ADAM as mentioned in Section 2.3 with initial learning rate 4×10^{-4} and L^2 regularisation weight decay rate 10^{-7} . The learning rate decays by half after every 50 epochs and the training process lasts for 500 epochs. We show the training results of $\tau_{\text{midpoint}} = 1$ case in Figure 3. Figure 3(a) shows the loss curve on the training and testing datasets throughout the training process, while 3(b) compares the neural network prediction with the numerical solution given by the implicit midpoint method with time step $\tau = 1$ solved by Newton's method. It is noteworthy that in Figure 3(b), the tested initial data is also generated by (17) but lies out of training and testing datasets. The L^2 error of the prediction here is lower than 1.67×10^{-3} , which

indicates the efficiency of the Neural Network approximation to the one step implicit method even with a relatively large time step such as 1.

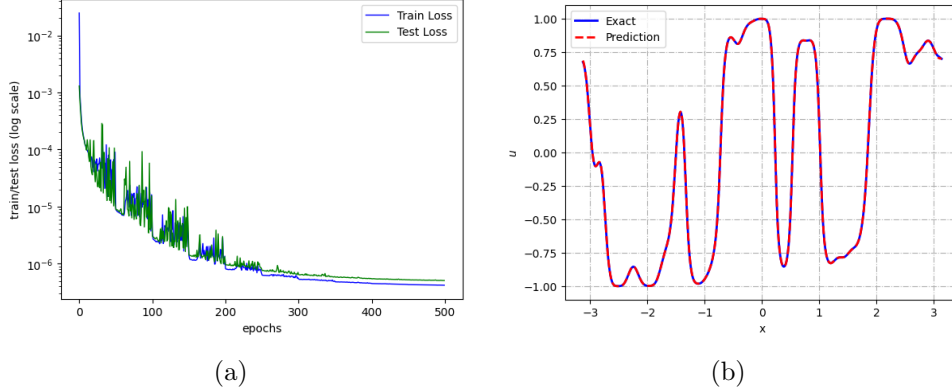


Figure 3: (a) Loss curve; (b) Comparison between neural network prediction and exact midpoint solution

In the following, we use the neural network prediction as the initial guess in Newton's method to solve (8) until steady state and compare the performance of our neural hybrid solver with one explicit solver, the ETD scheme, with different time steps and two other Newton solvers – one with direct initial guess (the numerical solution from the former time step) and the other with ETD solution as the initial guess. In our implementation, all the calculations of the exponential function and φ_1 function in the ETD scheme are accelerated by the standard Krylov method with generating only 10 basis vectors in the Arnoldi iteration.

To begin with, we check the convergence and the iteration count of Newton iteration using three different initial guesses in solving one step of the implicit midpoint method. Figure 4 exhibits how the update size changes in the iteration. As we can see from the plot, the neural network prediction can provide an initial guess that is much closer to the solution compared to the direct initial guess and the ETD solution with the same time step, which leads to a reduction in iteration count. Furthermore, to eliminate the impact of randomness in initial values, we randomly generate 100 different initial data and estimate the average iteration count. The result is shown in Table 1.

Then we consider multiple time steps of the implicit midpoint method and solve the equation until $T = 4$. We first plot the CPU time versus the

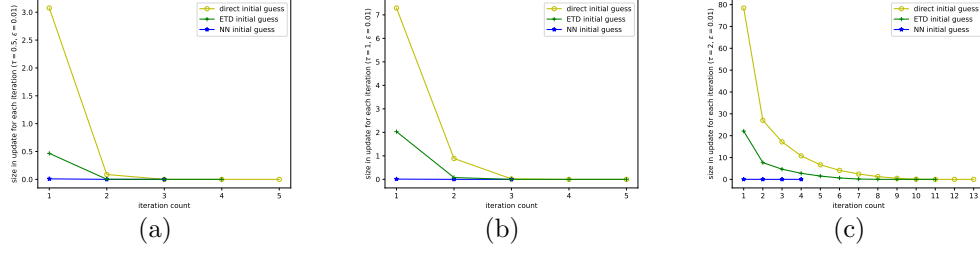


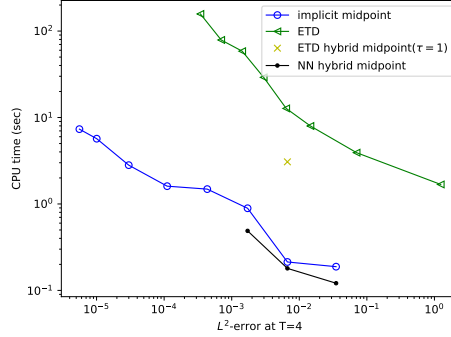
Figure 4: Update size VS iteration count (1D). The yellow line represents iteration with direct initial guess, the blue line represents iteration with NN prediction initial, and the green line represents iteration with ETD solution initial. (a) $\tau_{midpoint} = 0.5$; (b) $\tau_{midpoint} = 1$; (c) $\tau_{midpoint} = 2$.

Iteration Count \ Initial Guess	Direct initial	ETD ($\tau = \tau_{midpoint}$)	NN prediction
$\tau_{midpoint}$			
0.5	5.00	4.00	3.02
1	5.00	5.00	3.18
2	12.10	9.57	4.25

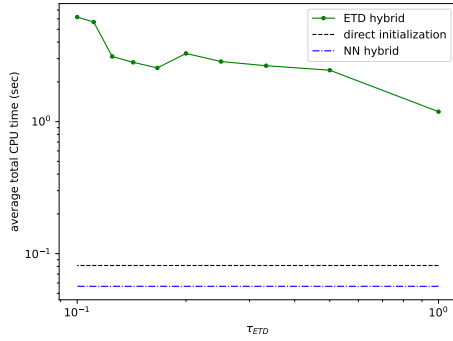
Table 1: Average iteration count in one time step using different initial guess (1-dimensional)

L^2 error of solutions at $T = 4$ using the implicit midpoint method and the ETD scheme in Figure 5(a). To achieve the same accuracy, the implicit midpoint method requires less computational time than the ETD scheme. When $\tau_{midpoint} = 1$, the L^2 error of the midpoint method solution using direct initial guess is 6.67×10^{-3} and the corresponding CPU time is 0.21 (sec). The neural hybrid solver reduces the CPU time to 0.18 (sec) without changing the accuracy, which accelerates the whole computation by 14.29%. The same results are observed in the cases when $\tau_{midpoint} = 0.5$ and 2 where our neural hybrid solver accelerates the midpoint method by 44.94% and 36.84%, respectively. We summarise the result of CPU time of direct initial solver and neural hybrid solver in Table 3 which can be found on page 34 in order to allow for comparison to the 2-dimensional case. ETD scheme, although it can also produce a "better" initial guess compared to the direct initial guess, fails to speed up the algorithm because of the high computational cost of its own. To further investigate whether the ETD solution with smaller time steps is capable of decreasing iteration count and the CPU time, we fix $\tau_{midpoint} = 1$ and consider a single time step midpoint method equipped with three Newton solvers. We vary τ_{ETD} in the ETD hybrid solver from 1 to 0.1. The green line with dot-markers in Figure 5(b) shows the CPU time (average results of 100 different initial data) of the ETD hybrid solver. The two benchmarks are CPU time using direct initial guess (black line) and the neural network predicted initial guess (blue line). Note that in this single time step, the CPU time for direct initial guess is 8.13×10^{-2} (sec), while the neural hybrid solver costs only 5.66×10^{-2} (sec) which speeds up one step of the implicit method by 30.38%. However, the CPU time for the ETD hybrid solver is always higher than the two benchmarks. Figure 5(c) exhibits the L^2 error of the three types of initial guesses. Combining the analysis in Figure 5(b) and Figure 5(c), a straightforward observation here is that if we keep decreasing τ_{ETD} in the ETD hybrid solver, the CPU time will increase since the calculation of initial guess should be more and more expensive.

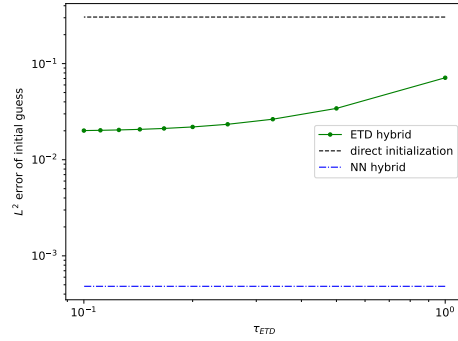
Finally, we investigate in Figure 6 the structure-preserving properties of the proposed neural hybrid solver. As shown in Figure 6(a), the ETD scheme with $\tau_{midpoint} = 2$ is unable to preserve the energy dissipation of the solution, whereas the hybrid solver with $\tau_{midpoint} = 0.5, 1, 2$ are all able to preserve this property. The maximum absolute value of solution $\max(|u|)$ is plotted in Figure 6(b). We observe that the ETD scheme with $\tau_{ETD} = 1$ and 2 fails to preserve the MBP, while the hybrid solver with $\tau_{midpoint} = 0.5$ and 1 appears to perfectly preserve this property until $T = 4$. Even though the



(a)



(b)



(c)

Figure 5: (a) CPU time VS the L^2 error. The green line represents the performance of ETD scheme, the blue line represents the midpoint method, the black line and the yellow cross are the result of NN hybrid and ETD hybrid solvers, respectively; (b) average CPU time in a single time step when ETD solutions with different time steps are used as the initial guess. The green line shows the average CPU time of ETD scheme, the black and blue lines represent the CPU time of direct initial guess and the NN hybrid method, respectively. Here, we fix $\tau_{midpoint} = 1$. (c) L^2 error of initial guesses when τ_{ETD} varies from 0.1 to 1. Here, $\tau_{midpoint} = 1$.

hybrid solver with time step 2 also fails to bound the solution in $[-1, 1]$, it still outperforms the ETD scheme with $\tau_{ETD} = 1$.

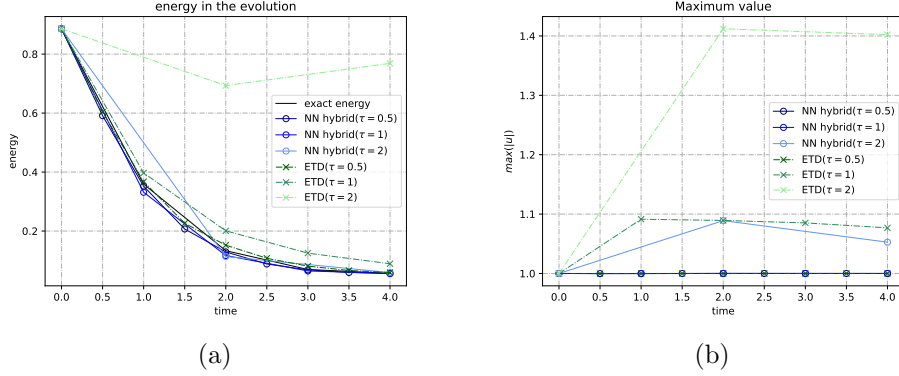


Figure 6: (a) energy of the solution calculated by ETD and neural hybrid solver; (b) maximum absolute value of the solution calculated by ETD and neural hybrid solver.

4.2. 2-dimensional example

We now evaluate the proposed method's ability to deal with 2-dimensional problems. The interfacial width ε is set to 0.02. The 128×128 uniform mesh is applied to discretise the 2D space domain $\Omega = [-\pi, \pi]^2 \subset \mathbb{R}^2$. The initial data u_0 in this example are generated as follows.

$$u_0(x_1, x_2) = \sum_{i=1}^{M_1} \sum_{j=1}^{M_2} [a_{ij} \sin(ix_1) \sin(jx_2) + b_{ij} \sin(ix_1) \cos(jx_2) + c_{ij} \cos(ix_1) \sin(jx_2) + d_{ij} \cos(ix_1) \cos(jx_2)],$$

where $a_{ij}, b_{ij}, c_{ij}, d_{ij} \sim \mathcal{N}(0, 1)$ are real coefficients randomly sampled from the normal distribution. Similar to the 1-dimensional case, all the initial data are normalised such that $u_0 \leftarrow \|u_0\|_{L^\infty} \leq 1$. We randomly generate 3520 different initial data and separate them into the training dataset $\{u_0^{(i)}\}_{i=1}^{N=3200}$ and testing dataset $\{u_0^{(i)}\}_{i=1}^{320}$.

The hyperparameter setting in this example is given as follows. 6 convolutional layers with one *Conv2d* operator and the activation function $\sigma =$

$\tanh()$ inside each layer are applied in our neural network model. All the *Conv2d* operators are equipped with the kernel size (9, 9), stride size (1, 1), padding size (4, 4) and the *reflect* padding mode. With this setting, the entire network has 417473 learnable parameters.

The constructed network is then trained by ADAM optimizer to approximate the implicit midpoint time-stepper with $\tau_{midpoint} = 0.25, 0.5, 1$. The learning rate starts from 4×10^{-4} and decays by half after every 50 epochs until 500 epochs. The L^2 regularisation weight decay rate is fixed to 10^{-7} . We first visualize the training result of the above-described neural network. Figure 7 displays the performance of neural time-stepper with $\tau_{midpoint} = 0.5$. Figure 7(a) shows the training and testing loss throughout 500 epochs, and Figure 7(b) compares the network prediction to the exact solution of the implicit midpoint stepper with $\tau_{midpoint} = 0.5$. The trained neural time-stepper achieves an L^2 absolute error lower than 1.90×10^{-3} .

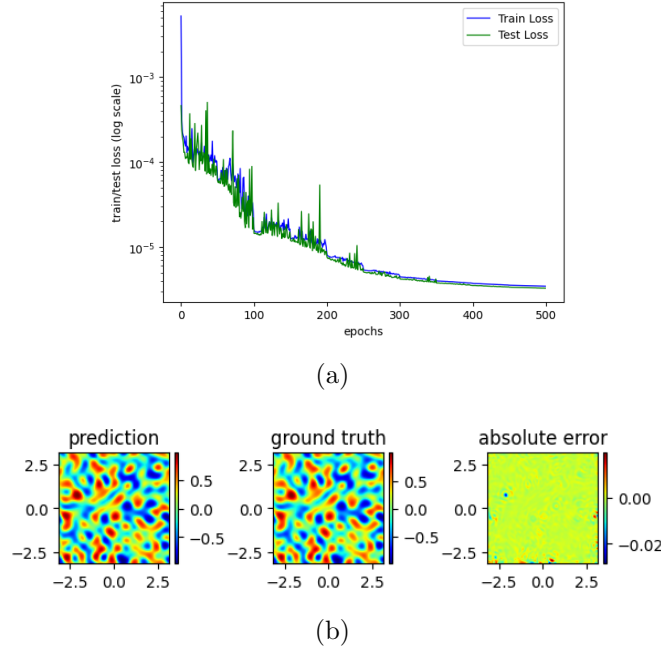


Figure 7: (a) Loss curve; (b) comparison between prediction and exact midpoint solution

The neural hybrid solver is then investigated in solving this 2-dimensional problem. We still compare its behaviour with the explicit ETD scheme. With

the help of the standard Krylov method, the size of discrete function value vector is reduced from 128^2 to 16 in approximating phi-functions, which vastly alleviates the cost of the ETD method.

We start again with solving a single step in the implicit midpoint method by Newton's method with three different initial guesses. Figure 8 exhibits the update size in the iteration. Notice that the dissipation of the update size indicates the convergence of the Newton's iteration. As shown in the plot, both the neural network prediction and the ETD solution with $\tau_{ETD} = \tau_{midpoint}$ offer better initial guesses and are capable of reducing iteration count when the time step is relatively large. We also display the result of the average iteration count over 10 different initial data in Table 2. Notice that, when $\tau_{midpoint} = 0.25$ the CPU time for direct initial guess, NN initial guess and ETD initial guess are 33.74, 27.64, 48.62 (sec), respectively. Thus, although the neural hybrid solver fails to reduce the iteration count in this case, it can still accelerate the algorithm by 18.08%. Since we use GMRES for the solution of the linear systems in Newton's iteration we suspect that this means the Krylov subspaces generated by the Neural Network initial guess provide a better approximation to the true solution value of the midpoint rule than the Krylov subspaces generated by either alternative initial guess. The multiple-time-steps result in Figure 9(a) further supports this conclusion.

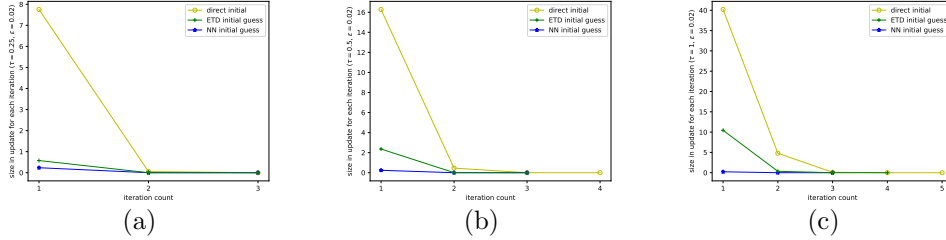


Figure 8: Update size VS iteration count (2D). The yellow line represents iteration with direct initial guess, the blue line represents iteration with NN prediction initial, and the green line represents iteration with ETD solution initial. (a) $\tau_{midpoint} = 0.25$; (b) $\tau_{midpoint} = 0.5$; (c) $\tau_{midpoint} = 1$.

We then examine the performance in multiple time steps of the three implicit time steppers and one explicit time stepper. Figure 9(a) shows the CPU time required to achieve a given L^2 error at $T = 5$ for both the implicit midpoint method and the ETD scheme. Generally speaking, the implicit

Iteration Count	Initial Guess	Direct initial	ETD ($\tau = \tau_{midpoint}$)	NN prediction
$\tau_{midpoint}$				
0.25		3.00	3.00	3.00
0.5		4.00	3.00	3.00
1		5.00	4.00	3.00

Table 2: Average iteration count in one time step using different initial guess (2-dimensional)

midpoint method is more computationally efficient than the ETD scheme if the same accuracy is required. The black line with dot-markers indicates that our neural hybrid solver accelerates the algorithm by 4.99%, 33.70%, and 33.90% when we consider time steps $\tau_{midpoint} = 0.25, 0.5$ and 1. The results of CPU time and acceleration rate are also exhibited in Table 3. As displayed by the yellow cross in Figure 9(a), the ETD hybrid solver increases the CPU time of the implicit midpoint method. To further explore whether the reduction in iteration count can compensate the cost of computing a better initial guess by choosing a smaller τ_{ETD} , we fix $\tau_{midpoint}$ to be 0.5 and vary τ_{ETD} from 0.05 to 0.5 in the ETD hybrid solver for a single time step. The outcomes in Figure 9(b) and 9(c) show that although decreasing τ_{ETD} leads to an improvement in initialisation, this advantage is offset by the increase in CPU time required in the ETD hybrid solver.

Test case	$\tau_{midpoint}$	Direct initial guess	Neural hybrid	Acc. Rate
1D	0.5	0.89	0.49	44.94%
	1	0.21	0.18	14.29%
	2	0.19	0.12	36.84%
2D	0.25	50.26	47.75	4.99%
	0.5	52.23	34.63	33.70%
	1	39.79	26.30	33.90%

Table 3: CPU time (sec) required for solving equation (8) until T. The acceleration rate of neural hybrid solver is shown in the last column. In 1D case, $T = 4$; in 2D case, $T = 5$.

The structure-preserving properties of the neural hybrid solver and ETD scheme are visualized in Figure 10. Figure 10(a) shows even though all the solvers can preserve energy dissipation, the neural hybrid solver has a higher energy accuracy than the ETD scheme. We witness in Figure 10(b) that the

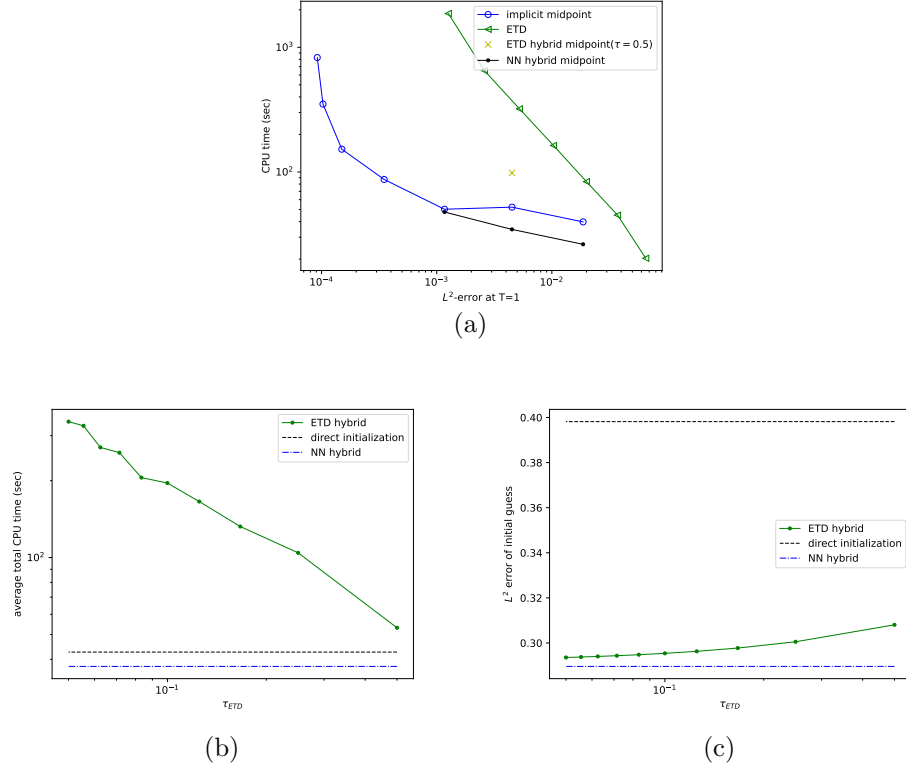


Figure 9: (a) CPU time VS the L^2 error. The green line represents the performance of the ETD scheme, the blue line represents the midpoint method, the black line and the yellow cross are the result of NN hybrid and ETD hybrid solvers, respectively; (b) average CPU time in a single time step when ETD solutions with different time steps are used as the initial guess. The green line shows the average CPU time of the ETD scheme, the black and blue lines represent the CPU time of direct initial guess and the NN hybrid solver, respectively. Here, we fix $\tau_{midpoint} = 0.5$; (c) L^2 error of initial guess when τ_{ETD} varies from 0.05 to 0.5. Here, $\tau_{midpoint} = 0.5$.

ETD scheme with $\tau_{ETD} = 1$ fails to preserve the MBP, while all other solvers appear to preserve this property well until $T = 5$.

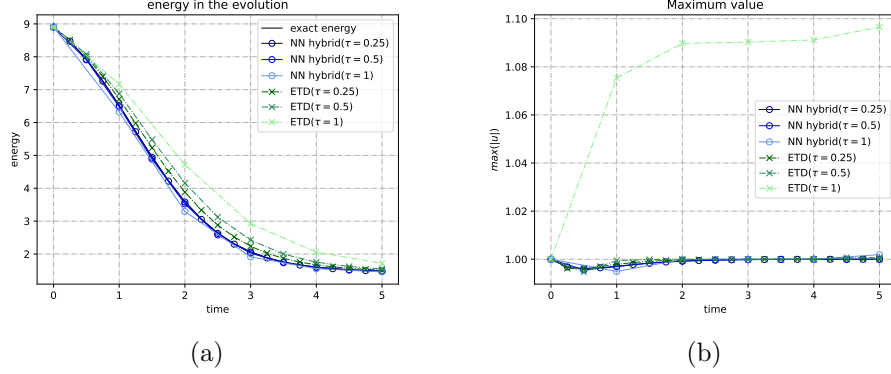


Figure 10: (a) energy of the solution calculated by the ETD and neural hybrid solver; (b) maximum absolute value of the solution calculated by the ETD and neural hybrid solver.

5. Conclusions and Discussions

In this work, we introduce a neural hybrid solver that accelerates Newton's method for implicit time stepping schemes using improved initialisation provided by a neural network. The neural time-stepper has the structure of a simplified CNN and is trained using a novel implicit-scheme-informed learning strategy. Consequently, it benefits from the advantages of being easy to implement, having fewer parameters leading to fast forward pass and, hence initialisation, and not requiring any labeled data for training. A quantifiable estimate of the reduction in the Newton iteration count for an improved initialisation is provided in Theorem 2, which indicates the advantage provided by a "good" initial guess in Newton's method. To illustrate the robustness of the proposed implicit-scheme-informed learning strategy, we prove in Theorem 3 that the generalisation error can be made arbitrarily close to the training error provided a sufficient amount of training data is used and in Proposition 1 we provide an upper bound on this number of training data required to achieve a desired accuracy in the generalisation error.

The efficiency of our proposed solver is demonstrated using several applications on solving Allen–Cahn equation equipped with homogeneous Neu-

mann boundary condition using the implicit midpoint method. Numerical implements, both in 1- and 2-dimensional settings, show that the neural hybrid solver outperforms other solvers in terms of accuracy, computational cost and structure-preservation. We remark that all the experiments displayed are completed on a pure CPU device after the neural network is trained. We found in our further exploration that given an input data, especially high dimensional data, the time for neural network prediction can be accelerated a lot if it is conducted on GPU devices. This suggests that there is significant potential to extend the neural hybrid solver to a wide range of high dimensional problems in future work.

A further direction for future work is the deeper understanding of the number of training data points required in the present set-up. Indeed, while Proposition 1 provides a reasonable upper bound for this, our numerical experiments indicate that good performance of our methodology is already achieved with a training dataset of more moderate size.

Acknowledgements

The authors would like to thank Qinyan Zhou (Sorbonne Université) for performing initial numerical studies that helped inform this research. Furthermore, the authors express their gratitude to Thibault Faney (IFP Energies Nouvelles), Antoine Lechevallier (IFP Energies Nouvelles & Sorbonne Université), and Frédéric Nataf (Sorbonne Université) for several helpful discussions. T.J. gratefully acknowledges funding from postgraduate studentship and Overseas Research Award of HKUST. K.S. gratefully acknowledges funding from the European Research Council (ERC) under the European Union’s Horizon 2020 research and innovation programme (grant agreement No. 850941). The work of Y.X. was supported by the Project of Hetao Shenzhen-HKUST Innovation Cooperation Zone HZQB-KCZYB-2020083. T.J. and Y.X. would like to thank HKUST Fok Ying Tung Research Institute and National Supercomputing Center in Guangzhou Nansha Sub-center for providing high performance computational resources.

References

- [1] E. Hairer, S. Nørsett, G. Wanner, Solving Ordinary Differential Equations II: Stiff and Differential-Algebraic Problems, Solving Ordinary Differential Equations II: Stiff and Differential-algebraic Problems, Springer, 1993.

- [2] R. Courant, K. Friedrichs, H. Lewy, Über die partiellen Differenzengleichungen der mathematischen Physik, *Mathematische Annalen* 100 (1928) 32–74.
- [3] C. G. Broyden, A class of methods for solving nonlinear simultaneous equations, *Mathematics of Computation* 19 (1965) 577–593.
- [4] E. S. Mehiddin Al-Baali, F. Maggioni, Broyden’s quasi-newton methods for a nonlinear system of equations and unconstrained optimization: a review and open problems, *Optimization Methods and Software* 29 (5) (2014) 937–954. doi:10.1080/10556788.2013.856909.
- [5] R. S. Dembo, S. C. Eisenstat, T. Steihaug, Inexact newton methods, *SIAM Journal on Numerical Analysis* 19 (2) (1982) 400–408. doi:10.1137/0719025.
- [6] L. Liu, W. Gao, H. Yu, D. E. Keyes, Overlapping multiplicative schwarz preconditioning for linear and nonlinear systems, *Journal of Computational Physics* 496 (2024) 112548. doi:https://doi.org/10.1016/j.jcp.2023.112548.
- [7] T. Chen, H. Chen, Universal approximation to nonlinear operators by neural networks with arbitrary activation functions and its application to dynamical systems, *IEEE Transactions on Neural Networks* 6 (4) (1995) 911–917. doi:10.1109/72.392253.
- [8] L. Lu, P. Jin, G. Pang, Z. Zhang, G. E. Karniadakis, Learning nonlinear operators via DeepONet based on the universal approximation theorem of operators, *Nature Machine Intelligence* 3 (3) (2021) 218–229.
- [9] Neural Operator: Graph Kernel Network for Partial Differential Equations.
- [10] Fourier Neural Operator for Parametric Partial Differential Equations.
- [11] L. Luo, X.-C. Cai, PIN[†]: Preconditioned inexact newton with learning capability for nonlinear system of equations, *SIAM Journal on Scientific Computing* 45 (2) (2023) A849–A871. doi:10.1137/22M1507942.
- [12] A. Lechevallier, S. Desrozier, T. Faney, E. Flauraud, F. Nataf, Hybrid Newton method for the acceleration of well event handling in the

simulation of CO2 storage using supervised learning, working paper or preprint (Apr. 2023).

- [13] J. Aghili, E. Franck, R. Hild, V. Michel-Dansac, V. Vigon, Accelerating the convergence of newton’s method for nonlinear elliptic pdes using fourier neural operators (2024). [arXiv:2403.03021](#).
- [14] G. Tierra, F. Guillén-González, Numerical Methods for Solving the Cahn–Hilliard Equation and Its Applicability to Related Energy-Based Models, *Archives of Computational Methods in Engineering* 22 (2) (2015) 269–289.
- [15] F. Guillén-González, G. Tierra, Second order schemes and time-step adaptivity for Allen–Cahn and Cahn–Hilliard models, *Computers & Mathematics with Applications* 68 (8) (2014) 821–846. doi:<https://doi.org/10.1016/j.camwa.2014.07.014>.
- [16] H. Gomez, T. J. Hughes, Provably unconditionally stable, second-order time-accurate, mixed variational methods for phase-field models, *Journal of Computational Physics* 230 (13) (2011) 5310–5327.
- [17] D. Hou, L. Ju, Z. Qiao, Energy-dissipative spectral renormalization exponential integrator method for gradient flow problems, *arXiv preprint arXiv:2310.00824* (2023).
- [18] S. Mishra, R. Molinaro, Estimates on the generalization error of physics-informed neural networks for approximating PDEs, *IMA Journal of Numerical Analysis* 43 (1) (2022) 1–43.
- [19] A. Alguacil, W. G. Pinto, M. Bauerheim, M. C. Jacob, S. Moreau, Effects of boundary conditions in fully convolutional networks for learning spatio-temporal dynamics, in: *Machine Learning and Knowledge Discovery in Databases. Applied Data Science Track*, Springer International Publishing, Cham, 2021, pp. 102–117.
- [20] A. Paszke, S. Gross, F. Massa, A. Lerer, J. Bradbury, G. Chanan, T. Killeen, Z. Lin, N. Gimeshein, L. Antiga, A. Desmaison, A. Köpf, E. Yang, Z. DeVito, M. Raison, A. Tejani, S. Chilamkurthy, B. Steiner, L. Fang, J. Bai, S. Chintala, *PyTorch: an imperative style, high-performance deep learning library*, Curran Associates Inc., 2019.

- [21] Adam: A Method for Stochastic Optimization.
- [22] E. Süli, D. F. Mayers, An Introduction to Numerical Analysis, Cambridge University Press, 2003.
- [23] R. A. Adams, J. J. Fournier, Sobolev Spaces, Academic Press, 1975.
- [24] S. Shalev-Shwartz, S. Ben-David, Understanding Machine Learning - From Theory to Algorithms., Cambridge University Press, 2014.
- [25] Intriguing properties of neural networks.
- [26] S. M. Allen, J. W. Cahn, A microscopic theory for antiphase boundary motion and its application to antiphase domain coarsening, *Acta Metallurgica* 27 (6) (1979) 1085–1095. doi:[https://doi.org/10.1016/0001-6160\(79\)90196-2](https://doi.org/10.1016/0001-6160(79)90196-2).
- [27] T. Tang, J. Yang, Implicit-explicit scheme for the allen-cahn equation preserves the maximum principle, *Journal of Computational Mathematics* 34 (5) (2016) 451–461.
- [28] Q. Du, L. Ju, X. Li, Z. Qiao, Maximum bound principles for a class of semilinear parabolic equations and exponential time-differencing schemes, *SIAM Review* 63 (2) (2021) 317–359. doi:[10.1137/19M1243750](https://doi.org/10.1137/19M1243750).
- [29] T. Gökler, Rational Krylov subspace methods for phi-functions in exponential integrators, Ph.D. thesis, Karlsruher Institut für Technologie (KIT) (2014). doi:[10.5445/IR/1000043647](https://doi.org/10.5445/IR/1000043647).